Hindawi
Shock and Vibration
Volume 2020, Article ID 3402168, 17 pages
https://doi.org/10.1155/2020/3402168

Research Article

Endocrine Composite Skyhook-Groundhook Control of Electromagnetic Linear Hybrid Active Suspension

Farong Kou, Qiangqiang Jing, Chen Chen, and Jianghao Wu

School of Mechanical Engineering, Xi'an University of Science and Technology, Xi'an 710054, China

Correspondence should be addressed to Farong Kou; koufarong@xust.edu.cn

Received 21 November 2019; Revised 7 January 2020; Accepted 17 January 2020; Published 29 February 2020

Academic Editor: Davood Younesian

In order to effectively improve vehicle riding comfort, handling stability, and realize vibration energy recovery, a new kind of electromagnetic linear hybrid active suspension (EMLHAS) integrated with linear motor and solenoid valve shock absorber is put forward. Firstly, for the analysis of the suspension performance, a quarter dynamic model of EMLHAS is established. At the same time, the mathematical models of a linear motor, including the active state and energy-regenerative state, are found. The correctness of mathematical models for the linear motor in the active and energy-regenerative states is verified by means of characteristic tests. Moreover, the velocity characteristic tests of solenoid valve shock absorber are carried out to determine its mathematical polynomial model in the semiactive state. Then, a new kind of multimode endocrine composite skyhook-groundhook control strategy is proposed. The suspension motion is divided into four modes according to the driving conditions of the vehicle. An endocrine control with long feedback and short feedback is combined with the skyhook-groundhook control. The control laws of the skyhook-groundhook controller and endocrine controller are, respectively, designed. Finally, the simulation analysis of suspension dynamic performance and energy-regenerative characteristic is done. The results show the control effect of endocrine composite skyhook-groundhook control is better than that of skyhook-groundhook control, which improves vehicle riding comfort and handling stability. Moreover, part of vibration energy is recovered.

1. Introduction

Active suspension can effectively improve vehicle riding comfort and handling stability by outputting active force of the actuator [1–3]. However, the active suspension actuator needs to consume a large amount of external energy and it reduces the economic performance of the vehicle [4–7].

In recent years, domestic and overseas scholars have been studying on how to reduce the energy consumption of the active suspension, while ensuring dynamic performance of the vehicle [8–11]. Among them, many scholars put forward the hybrid suspension systems with different working modes so as to coordinate the contradictions between dynamic performance and energy consumption of the suspension system. For example, in [12], a hybrid electromagnetic suspension with three modes was proposed and the influences of the stiffness and damping on suspension dynamics and energy consumption were analyzed. The experimental results indicate that the hybrid electromagnetic suspension can reduce the energy consumption under the active control. In [13], a parallel composite electromagnetic suspension with an electromagnetic actuator and magnetorheological damper was proposed and a multimode switching controller based on model reference was designed. The results show that the switching controller can effectively switch between different working modes, which balance the contradiction between vibration attenuation and energy recovery.

At the same time, the contradiction between vehicle riding comfort and handling stability under the single working mode of the suspension system has always existed. Therefore, scholars have carried out research on the control strategies of different working modes of the suspension system, focusing on how to improve suspension performance under corresponding working modes. Skyhook control mainly improves vehicle riding comfort [14–16], while groundhook control mainly improves vehicle handling stability [17, 18]. The skyhook-groundhook control takes

into account the advantages of both skyhook control and groundhook control, and the dynamic performance in different working modes can be improved by allocating the skyhook damping coefficient and groundhook damping coefficient. For example, in [19], it comprehensively considered the safety and riding comfort, in research of restraining lateral vibration of high-speed rail vehicles. The effects of the skyhook-groundhook damping control were studied. The results show that the damping control of the skyhook-groundhook exhibits better comprehensive performance by adjusting the damping coefficients of the skyhook-groundhook control.

As for the research of the skyhook-groundhook control strategy, many scholars focus on the given parameters of the suspension system seldom consider the control effects of the suspension system under the changing parameters. When the vehicle system runs on an uneven road, it is inevitable to suffer from uncertainties such as sprung mass and tire stiffness, so the suspension controller should be adaptive to these complex and uncertain environment. In recent years, the endocrine control has been widely studied in various fields because of its excellent adaptive performance and self-learning ability [20–22]. In [23], an endocrine single-neuron PID compound sliding control system was designed; the output gain of whole order neuron PID was controlled by using a fuzzy controller. The results show that the controller with endocrine variable gain single-neuron sliding has better performance than the traditional PID controller. In [24], an endocrine LQR control strategy was proposed and applied to the active suspension system. The simulation results show that the endocrine LQR control was better than the traditional LQR control, still had good adaptability under the simulation of changing parameters.

In this paper, a new kind of electromagnetic linear hybrid active suspension (EMLHAS) system integrated with linear motor and solenoid valve shock absorber is put forward. The EMLHAS actuator can work in different states, according to the suspension controller, so as to recover vibration energy, while ensuring vehicle riding comfort and handling stability. In Section 3, the mathematical models of different states for the linear motor are found; the characteristic tests are carried out to verify the correctness of mathematical models. Moreover, velocity characteristic tests of the solenoid valve shock absorber are carried out to determine its mathematical polynomial model in the semiactive state. In Section 4, the suspension motion is divided into four modes according to the driving conditions of the vehicle. A new multimode endocrine composite skyhook-groundhook control strategy is designed and applied. In Section 5, the simulation analysis of the suspension dynamic performances in time domain and frequency domain is done and the energy-regenerative characteristics are analyzed as well.

2. Structure and Principle of the EMLHAS System

The structure of the EMLHAS system is shown in Figure 1. The system mainly consists of an EMLHAS actuator, spiral spring, super capacity, battery, suspension controller, corresponding signal detection device, and so on. The suspension motion is divided into four modes, namely, economy, safety, comfort, and comprehensive, respectively. When the vehicle is running on an uneven road, the suspension controller can make the EMLHAS actuator work in the active state, energy-regenerative state, or semiactive state according to the external conditions under different modes and then outputs the corresponding control force with the signals detected by relevant sensors.

The structure of the EMLHAS actuator is shown in Figure 2, which mainly consists of linear motor, solenoid valve shock absorber, upper ear, and lower ear. The linear motor can work in the active state or the energy-regenerative state, and the solenoid valve shock absorber can work in the semiactive state.

The linear motor and solenoid valve shock absorber work in different states under different modes, which mainly includes two cases. Under the economy mode, the road condition is good; in order to reduce energy consumption, the solenoid valve shock absorber works in the semiactive state to generate damping force to attenuate vibration; the desired ideal force is acquired from the endocrine composite skyhook-groundhook control by a suspension controller. The controllable current is inputted to generate the real damping force to attenuate vibration according to the ideal force. Meanwhile, the linear motor works in the energy-regenerative state and the counter-electromotive force (CEMF) is generated through cutting the magnetic induction line, and then electric energy is stored in the super capacity to realize the vibration energy recovery.

Under the other three modes, the road condition is worse; the linear motor works in the active state to generate active force to attenuate vibration; the desired force is acquired from the endocrine composite skyhook-groundhook control by a suspension controller. The controllable current is inputted to the linear motor to generate the real active force to attenuate vibration according to the ideal force. At the same time, the hydraulic damping force generated by the solenoid valve shock absorber hinders the movement of the linear motor because they are connected in series structure, so the solenoid valve shock absorber is energized to work in the semiactive state to reduce hydraulic damping force.

3. Modeling of EMLHAS Dynamic Model

3.1. Dynamic Model of EMLHAS. In this paper, a quarter vehicle dynamic model of EMLHAS is established [25], which is shown in Figure 3.

According to Figure 3, based on Newton's laws of motion, the dynamic motion equations for the quarter vehicle suspension can be expressed as

$$\begin{cases} m_s\ddot{x}_s + k_s(x_s - x_u) + F = 0, \\ m_u\ddot{x}_u - k_s(x_s - x_u) + k_t(x_u - z) - F = 0. \end{cases} \tag{1}$$

The state variable and output vector are selected as follows:

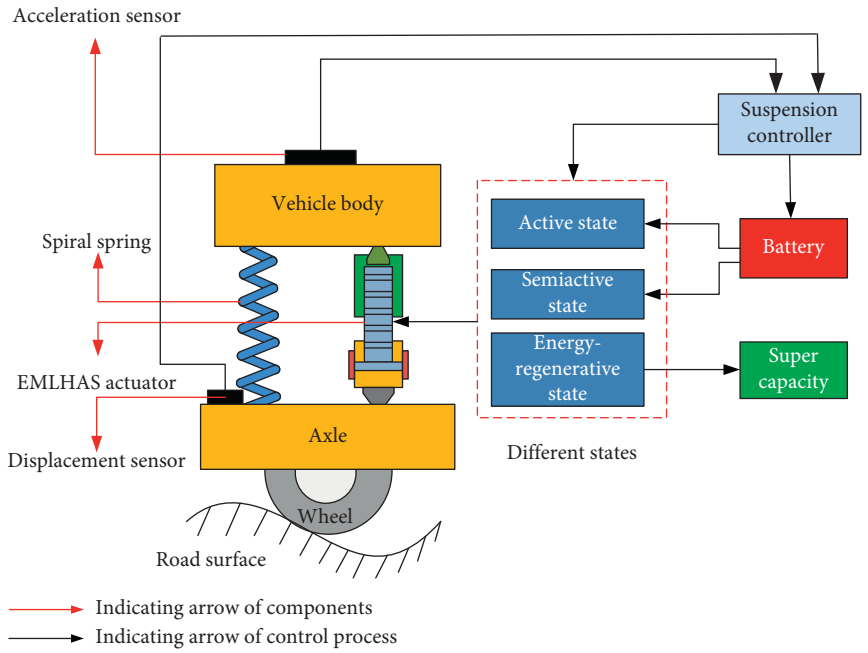

Figure 1: Structure of the EMLHAS system.

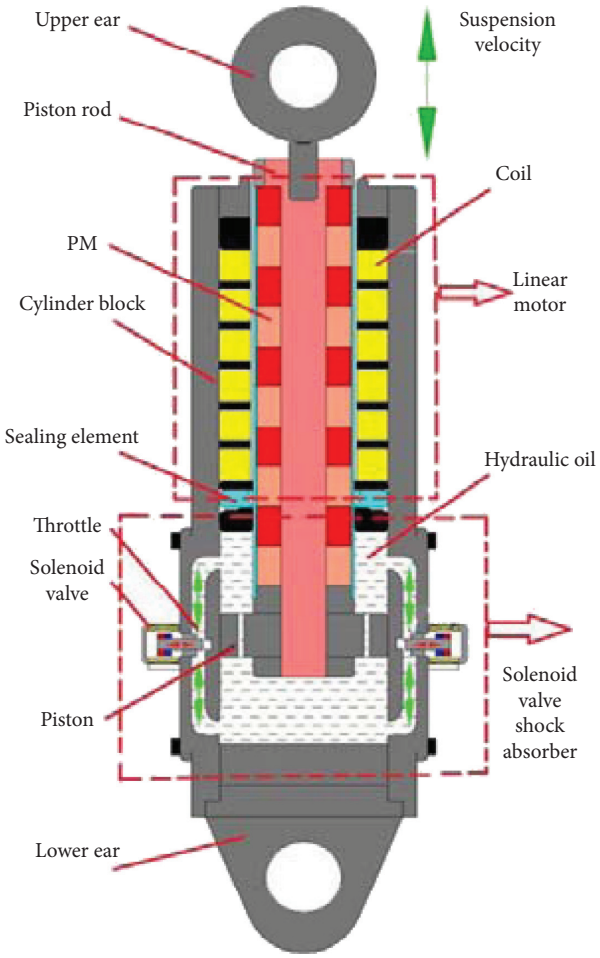

Figure 2: Structure of the EMLHAS actuator.

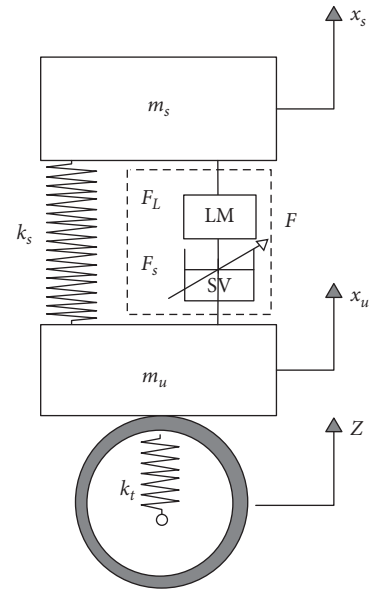

Figure 3: Dynamic model with 2-DOF of EMLHAS. LM, linear motor; SV, solenoid valve shock absorber.

$$\mathbf{X} = \left[x_s - x_u \quad \dot{x}_s \quad x_u - z \quad \dot{x}_u\right]^T,$$
$$\mathbf{Y} = \left[\ddot{x}_s \quad x_s - x_u \quad k_t\left(x_u - z\right) \quad \dot{x}_u\right]^T, \tag{2}$$

where m_s is the sprung mass, m_u is the unsprung mass, k_s is the spring stiffness coefficient, F is the control force of suspension (especially, F_L is the control force of the linear motor in the active state and F_s is the control force of the solenoid valve shock absorber in semiactive state), k_t is the tire stiffness coefficient, z is the displacement of road input,

x_s is the displacement of sprung mass, and x_u is the displacement of unsprung mass.

In this way, the state-space equations of suspension can be expressed as follows:

$$\begin{cases} \dot{X} = \mathbf{AX} + \mathbf{BU}, \\ \mathbf{Y} = \mathbf{CX} + \mathbf{DU}, \end{cases} \tag{3}$$

where A is the state matrix, B is the input matrix, C is the output matrix, and D is the transfer matrix. When the control input force F is 0, it becomes passive suspension:

$$\mathbf{A} = \begin{bmatrix} 0 & 1 & 0 & -1 \\ -\frac{k_s}{m_s} & -\frac{c_s}{m_s} & 0 & \frac{c_s}{m_s} \\ 0 & 0 & 0 & 1 \\ \frac{k_s}{m_u} & \frac{c_s}{m_u} & -\frac{k_t}{m_u} & -\frac{c_s}{m_u} \end{bmatrix},$$

$$\mathbf{B} = \begin{bmatrix} 0 & 0 \\ 0 & \frac{1}{m_s} \\ -1 & 0 \\ 0 & -\frac{1}{m_u} \end{bmatrix},$$

$$\mathbf{C} = \begin{bmatrix} -\frac{k_s}{m_s} & -\frac{c_s}{m_s} & 0 & \frac{c_s}{m_s} \\ 1 & 0 & 0 & 0 \\ 0 & 0 & k_t & 0 \\ 0 & 0 & 0 & 1 \end{bmatrix}, \tag{4}$$

$$\mathbf{D} = \begin{bmatrix} 0 & \frac{1}{m_s} \\ 0 & 0 \\ 0 & 0 \\ 0 & 0 \end{bmatrix},$$

$$\mathbf{U} = \begin{pmatrix} \dot{z} \\ F \end{pmatrix}.$$

A filtered white noise is adopted as the road surface input model [26]:

$$\dot{z}(t) = -2\pi f_0 z(t) + 2\pi\sqrt{G_0 u_0}\omega_0(t), \tag{5}$$

where G_0 is the road irregularity coefficient, f_0 is the lower cutoff frequency, u_0 is the vehicle speed, and $\omega_0(t)$ is the unit white noise. Among these parameters, the road irregularity coefficient and vehicle speed are the two main factors need to be considered. The road irregularity coefficient represents the road surface level; the road surface level and vehicle speed can constitute different driving conditions.

3.2. Mathematical Models of the EMLHAS Actuator. The mathematical models of the EMLHAS actuator include the linear motor mathematical model and solenoid valve shock absorber mathematical model. The mathematical models of a linear motor, including the active state and energy-regenerative state, are established. Also, force characteristic tests and energy-regenerative characteristic tests are carried out to verify the correctness of the mathematical models. Meanwhile, the solenoid valve shock absorber is one kind of semiactive suspension for its strong nonlinear factors in mathematical modeling; the mathematical model of the solenoid valve shock absorber is established through test modeling [27].

3.2.1. Modeling of Active State for Linear Motor and Force Characteristic Test Verification. When the linear motor works in the active state, the active force is generated by inputting controllable current to attenuate vibration.

The mathematical model of the linear motor is complicated to derive under the UVW coordinate system. In order to simplify the mathematical model and achieve the best control of it. The transformation of the two-phase stationary $\alpha - \beta$ coordinate system and the two-phase rotating $d - q$ coordinate system are carried out successively [28]. Then, the space vector relationship of the three coordinate systems is shown in Figure 4.

Finally, the state equation under the two-phase rotating $d - q$ coordinate system is obtained as [29]

$$\begin{cases} \dfrac{\mathrm{d}i_d}{\mathrm{d}t} = -\dfrac{R}{L_d} i_d + \dfrac{L_q}{L_d}\omega i_q + \dfrac{u_d}{L_d}, \\ \dfrac{\mathrm{d}i_q}{\mathrm{d}t} = -\dfrac{R}{L_q} i_q - \dfrac{L_d}{L_q}\omega i_d - \dfrac{\varphi_f}{L_q}\omega + \dfrac{u_q}{L_q}, \end{cases} \tag{6}$$

where R is the winding resistance, L_d is the direct axis inductance, L_q is the quadrature axis inductance, φ_f is the permanent magnet flux linkage, ω is the electrical angular velocity, i_d is the direct axis current, i_q is the quadrature axis current, u_d is the direct axis voltage, and u_q is the quadrature axis voltage.

The active force generated by the linear motor is expressed as

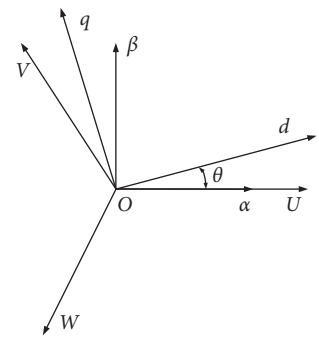

Figure 4: The relationship of the space vector for different coordinate systems. θ is the electrical angle in the coordinate transformation.

$$F_L = \frac{1.5 P_n \pi \varphi_f i_q}{\tau}, \tag{7}$$

where F_L is the active force generated by the linear motor, P_n is the pole logarithm, and τ is the pole distance.

The thrust coefficient of the active force for the linear motor is expressed as

$$K_i = \frac{3 P_n \pi \varphi_f}{2\tau}. \tag{8}$$

The mechanical motion equation of the linear motor is expressed as

$$M\frac{\mathrm{d}v}{\mathrm{d}t} = F_L - f_1 - Bv, \tag{9}$$

where M is the mass of moving parts, v is the velocity of moving parts, f_1 is the load, and B is the viscous damping coefficient.

The energy consumption power of the linear motor in the active state is used to represent the energy consumption characteristic of the EMLHAS system, which is expressed as

$$W = \int_0^t F_L \cdot \dot{x}_{s-u} \mathrm{d}t, \tag{10}$$

where $\dot{x}_{s-u}$ is the suspension velocity and W is the energy consumption power.

The correctness of the mathematical model in the active state is verified through the force characteristic tests of the linear motor in Figure 5. During the test, the linear motor is installed on the test bed. The upper end of the linear motor is connected with the upper crossbeam that is fixed on the test bed. The bottom end of the linear motor is connected with the bottom crossbeam that is connected with the vibration table. The three-phase alternating current is inputted through the TSGC2-6KVA three-phase voltage regulator to drive the linear motor, the LTR-1 force sensor is used to measure the active force signal generated by the linear motor, and DH5902 data acquisition instrument is used to collect the active force signals. Different input voltages are provided to the linear motor through the voltage regulator during the test; the input voltage of the linear motor is increased from 10 V to 50 V; three tests are conducted under

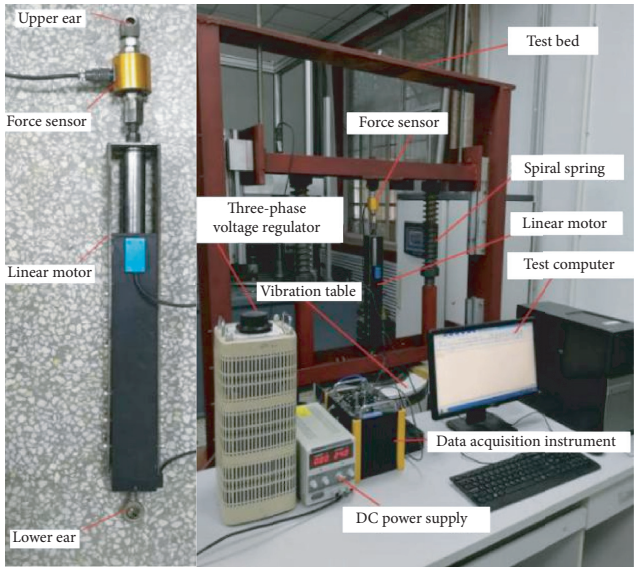

Figure 5: Force characteristic tests of the linear motor.

each voltage, and the average value is compared with the simulation value, and the results are listed in Table 1.

Table 1 shows that the input voltage increases from 10 V to 50 V; the average test values and simulation values of the active force are basically same, the error between them is within 4%-5%. When the input voltage of the linear motor is 50 V, the error between them is greatest. At this time, the average test value of active force is 378.69 N and simulation value is 398.21 N, the error between them is 4.9%. The main reason of error is that nonlinear factors are ignored while establishing the mathematical model of the linear motor. At the same time, self-weight factors, energy loss of all parts, and the precision of measuring equipment should be considered during the test. Finally, the correctness of the mathematical model in the active state is verified by using the comparative analysis of the simulation and force characteristic tests.

3.2.2. Modeling of Energy-Regenerative State for Linear Motor and the Test Verification. When the linear motor works in the energy-regenerative state, the CEMF is generated by cutting magnetic induction line of the linear motor and then charges the super capacity in the form of regenerative voltage [30]. The regenerative voltage is expressed as

$$U_r = K_e \dot{x}_{s-u}, \tag{11}$$

where U_r is the regenerative voltage and K_e is the CEMF coefficient of the linear motor.

The regenerative power of the linear motor is used to represent the energy-regenerative characteristic of the EMLHAS system, which is expressed as

$$P_r = U_r \cdot i_r = \frac{U_r^2}{R}, \tag{12}$$

where P_r is the regenerative power of the linear motor and i_r is the coil current of the linear motor in energy-regenerative state.

In order to verify the correctness of the mathematical model in the energy-regenerative state for the linear motor, the energy-regenerative characteristic tests of the linear motor are carried out in Figure 6. The linear motor is installed on the test bed. The vibration table can output vibration excitation to simulate road surface input; The test condition is at sinusoidal road in which the frequency is at 2 Hz and amplitude is at 10 mm and 15 mm,. The linear motor follows the up and down movement with the vibration table. Then, regenerative voltage charges the super capacity through a rectifier and bidirectional DC-DC converter to realize energy recovery. The regenerative voltage and regenerative power are tested. Based on the mathematical model of the energy-regenerative state, the simulation results are compared with the test results; the comparative results are shown in Figure 7.

Figure 7 shows that the results of test and simulation are basically consistent. For example, from test results, at the input of 2 Hz and 15 mm, the maximum regenerative voltage is 11.04 V and the average regenerative voltage is 6.53 V. The maximum regenerative power is 18.9 W and the average regenerative power is 10.83 W. The error between the average test value and the average simulation value is within 4%-5%; the main reason for the error between them is that the resistance in the energy-regenerative circuit generates energy consumption, so the loss of the power tube in the circuit is existed. The error is within the acceptable range, which indicates the correctness of the mathematical model for the linear motor in the energy-regenerative state. This shows that the EMLHAS system designed in this paper can achieve vibration energy recovery through the linear motor.

3.2.3. Test Modeling of Semiactive State for Solenoid Valve Shock Absorber. In order to obtain the mathematical model of the solenoid valve shock absorber, the test modeling is carried out in Figure 8. The solenoid valve shock absorber is installed on the test bed. The frequency is at 2 Hz and the amplitude is at 5 mm of the sinusoidal excitation from vibration table, which is taken as road input. The adjustable current by regulated DC power supply is inputted to the solenoid valve shock absorber and then the solenoid valve shock absorber is drived to generate the damping force. The damping force signals are measured by using a force sensor. Also, suspension displacement signals generated by the solenoid valve shock absorber are measured by using a displacement sensor. The collected signals are processed by data acquisition instrument. Finally, the regression fitting curves of velocity characteristics for the solenoid valve shock absorber are obtained under various control currents, as shown in Figure 9.

The damping force F_s of the solenoid valve shock absorber is expressed as

$$F_s = \sum_{k=0}^{3} \left(b_k I^2 + c_k I + d_k\right) \dot{x}_{s-u}^{\,k}, \tag{13}$$

where the values of k are 0, 1, 2, and 3; b_k, c_k, and d_k are polynomial coefficients; and I is control current of the solenoid valve shock absorber.

Table 1: Force characteristic test results of the linear motor.

Voltage (V)	Test values (N)				Simulation values (N)	Error (%)
	First test	Second test	Third test	Average values		
10	163.28	163.19	163.34	163.27	170.25	4.1
20	216.08	216.04	216.03	216.05	225.53	4.2
30	267.84	267.91	267.89	267.88	280.21	4.4
40	314.99	314.97	314.92	314.96	330.15	4.6
50	378.71	378.70	378.66	378.69	398.21	4.9

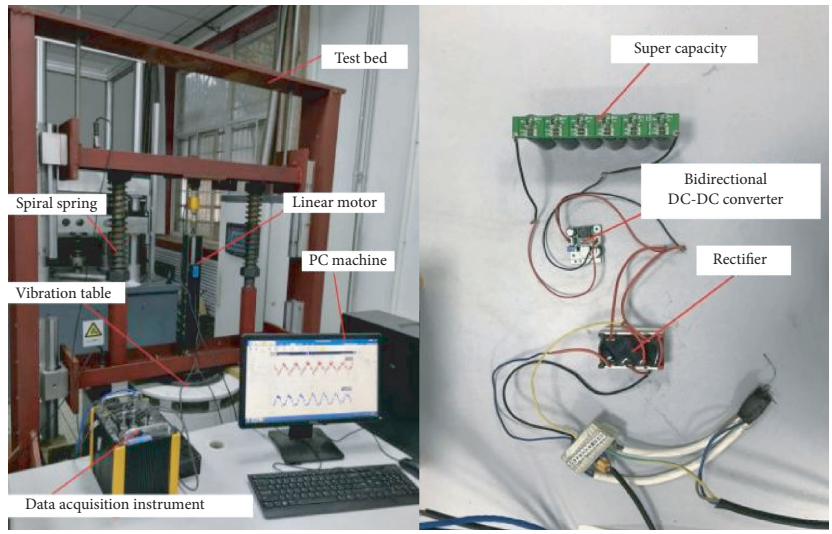

Figure 6: Energy-regenerative characteristic tests of the linear motor.

The parameters of the polynomial model for the solenoid valve shock absorber are identified by means of regression analysis. The polynomial coefficients are obtained as shown in Table 2. By taking the identified parameter results into equation (13), the polynomial model of the solenoid valve shock absorber can be obtained.

4. Multimode Endocrine Composite Skyhook-Groundhook Control Strategy

The driving conditions of vehicle speed and road surface are considered to divide the working modes of the EMLHAS system. The endocrine composite skyhook-groundhook control strategy is proposed, which is composed of endocrine control and skyhook-groundhook control. The control laws of the skyhook-groundhook controller and endocrine controller are, respectively, designed to improve the control effect. The multimode control block diagram of the EMLHAS system is shown in Figure 10.

The road driving conditions determine the working states of the EMLHAS actuator. Once the vehicle runs on the road, the driving conditions can be determined according to the vehicle speed and road surface. Then, the working mode of the suspension system is divided. Different working modes focus on the corresponding performance requirements; the EMLHAS actuator will be designed to work in the different states. Therefore, as long as the vehicle runs, the EMLHAS actuator makes different components (the linear motor and solenoid valve shock absorber) work in the corresponding states according to the design requirements.

4.1. Division of Suspension Working Modes Based on Driving Conditions. Different road input constitutes different driving conditions; the two main factors of road input are vehicle speed and road surface level. According to the actual road driving conditions, the vehicle speed is set at 0–80 km/h and the road surface level is from B level to D level. 40 km/h is set as the speed limit, and the C road surface level is set as the road surface limit. The driving conditions are divided into four quadrant regions, which are low speed with even road condition, high speed with uneven road condition, high speed with even road condition, and low speed with uneven road condition, respectively. Based on different driving conditions, the working modes of the suspension system are divided to meet the different performance requirements, namely, economy mode, safety mode, comfort mode, and comprehensive mode, respectively. Numerical value is used to represent the working states of the EMLHAS actuator. LM = 1 means the linear motor works in the active state, LM = 2 means the linear motor works in the energy-regenerative state, and SV = 1 means the solenoid valve shock absorber works in the semiactive state. Both the linear motor and solenoid valve shock absorber are controlled under different working modes. The specific division results and the EMLHAS actuator working states in each mode are as shown in Figure 11.

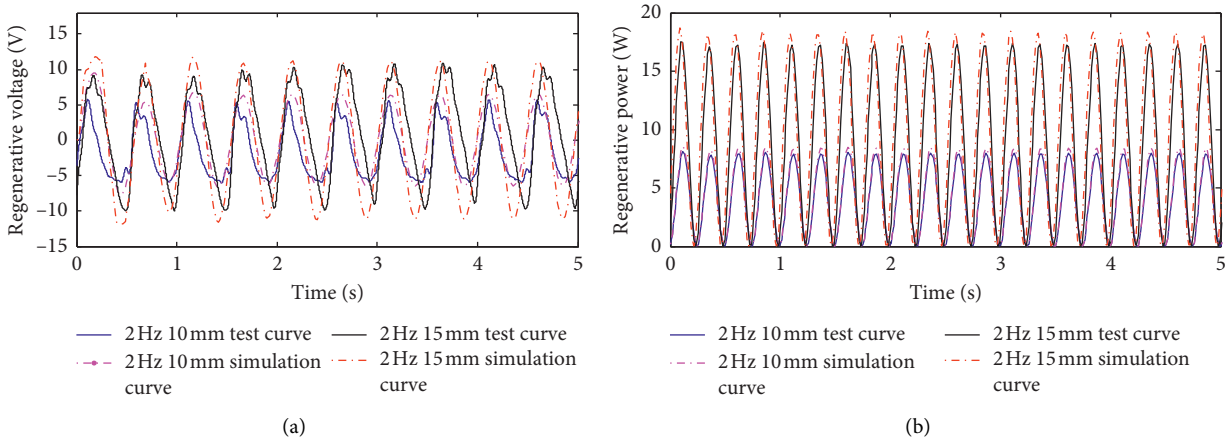

Figure 7: Result comparison between test and simulation. (a) The regenerative voltage. (b) The regenerative power.

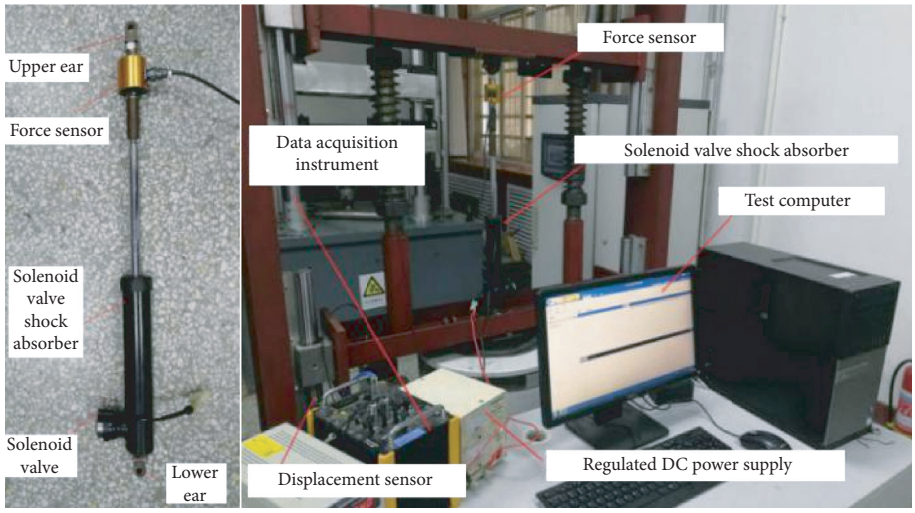

Figure 8: Velocity characteristic tests of the solenoid valve shock absorber.

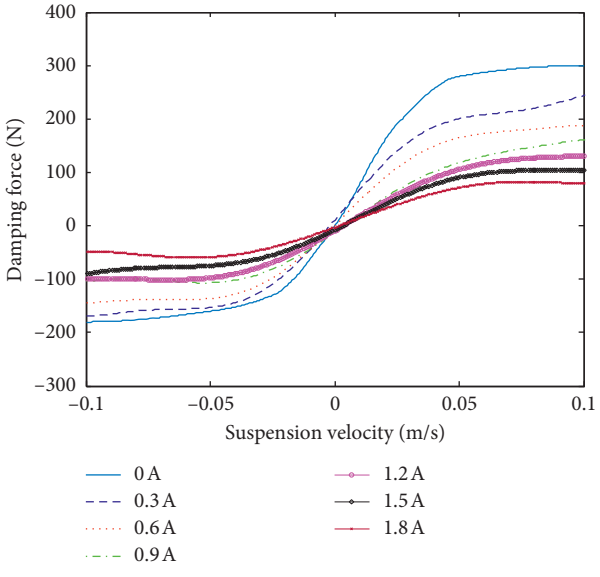

Figure 9: Regression fitting curves of velocity characteristic tests.

Table 2: Parameter identification results.

k	0	1	2	3
b_k	9614	8905	−81.0	−11.45
c_k	26240	−18980	−894.1	10.16
d_k	−95216	17288	2420.3	1.86

The driving condition is the best under the economy mode, which is with lower vehicle speed and better road surface level. The solenoid valve shock absorber works in the semiactive state to generate damping force F_s to attenuate vibration because the solenoid valve shock absorber is one kind of semiactive suspension, which can achieve a better effect on vibration attenuation with less energy consumption under good driving conditions. At the same time, the linear motor works in the energy-regenerative state to recover vibration energy, so both the suspension dynamic performance and the regenerative power of the linear motor are taken into account.

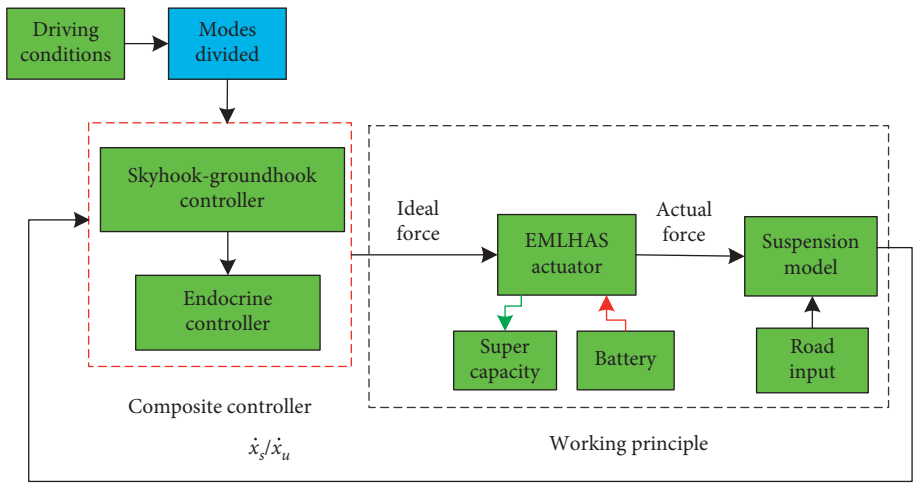

Figure 10: Multimode control block diagram of the EMLHAS system.

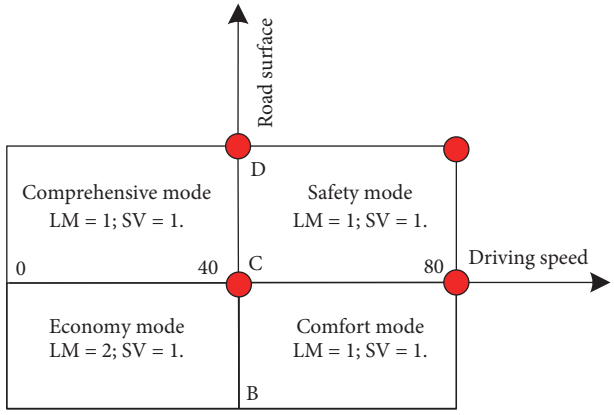

Figure 11: Division of suspension working modes based on driving conditions.

The corresponding performance indexes are also different under the other three working modes. The main index of the safety mode is dynamic tire load, the main index of the comfort mode is sprung mass acceleration, and the main index of the comprehensive mode takes into account both sprung mass acceleration and dynamic tire load. Under these three modes, driving condition is all worse than that under the economy mode, so the vibration attenuation is the main thing. The linear motor has a larger output power; the vibration attenuation effect in the active state is better than the semiactive of the solenoid valve shock absorber. Therefore, the linear motor is selected to work in the active state, to generate the active force F_L for vibration attenuation. At the same time, the linear motor and solenoid valve shock absorber structure are connected in series structure. When the linear motor works in the active state, the hydraulic damping force generated by the solenoid valve shock absorber is hindering linear motor vibration attenuation, which increases the energy consumption of the linear motor. Hence, the solenoid valve shock absorber will be energized to work in the semiactive state to reduce the hydraulic damping force, so as to reduce the energy consumption of the linear motor.

The working states of the EMLHAS actuator under the safety, comfort, and comprehensive mode are same. The linear motor works in the active state, and the solenoid valve shock absorber works in the semiactive state. Then, the EMLHAS system outputs corresponding active control force F_L to attenuate vibration. The highest vehicle speed and the worst road surface under different modes are selected from Figure 11. The typical working conditions are shown in Table 3.

4.2. Structure of Control System for Endocrine Composite Skyhook-Groundhook. This paper designs an endocrine composite skyhook-groundhook control strategy, which is based on the mechanism of hormone positive and negative feedback regulation from the three-stage loop of the hypothalamus-pituitary-endocrine gland for the biological endocrine system [31].

4.2.1. The Mechanism of Hormone Regulation in the Endocrine System. The hormone regulation mechanism is similar to the closed-loop feedback regulation mechanism in the control theory. Endocrine glands (thyroid, adrenal, gonad, and so on) secrete the corresponding hormones (thyroxine, adrenaline, testosterone, and so on) to regulate the body's metabolism. The specific process of hormone regulation is as follows.

The hypothalamus, pituitary, and endocrine glands make up the biological endocrine hormone regulating system. The feedback loop of the endocrine system includes long feedback and short feedback. The hypothalamus secreted pituitary hormone H1, and H1 stimulates the pituitary to secrete the endocrine gland-stimulating hormone H2, which in turn stimulates the endocrine glands to produce the corresponding hormone H3. This is the positive feedback regulation of hormone concentration H3. When the concentration of hormone H3 is too high, H3 in turn acts on the hypothalamus and pituitary gland to inhibit the secretion of corresponding hormones. This is negative feedback regulation. The positive and negative feedback regulation of

Table 3: The design of typical working condition for each mode.

Driving conditions	Modes division	Vehicle speed (km/h)	Road surface
Low speed with even road	Economy mode	40	C
High speed with uneven road	Safety mode	80	D
High speed with even road	Comfort mode	80	C
Low speed with uneven road	Comprehensive mode	40	D

hormone H3 on the hypothalamus and pituitary forms a long feedback loop. At the same time, the gland-stimulating hormone H2 released by the pituitary not only affects the endocrine glands but also affects the hypothalamus, forming a short feedback loop. The working principle is shown in Figure 12.

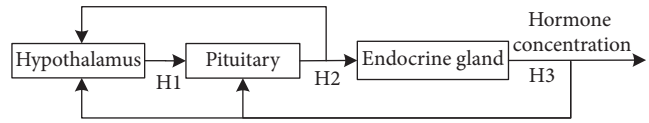

Figure 12: Hormone regulation loop of the endocrine system.

4.2.2. The Control System Structure for Endocrine Composite Skyhook-Groundhook. The control structure block diagram is shown in Figure 13, which is composed of the skyhook-groundhook controller and endocrine controller. The endocrine controller includes the long feedback control unit and the short feedback control unit; the long feedback control unit consists of the primary control unit and the secondary control unit.

In the endocrine controller, the primary control unit and the secondary control unit simulate the hypothalamus and pituitary, respectively. The direct feedback index is sprung mass acceleration. The short feedback control unit simulates the short feedback loop of the pituitary-hypothalamus in the biological endocrine system because the feedback index from the pituitary to the hypothalamus is distributed by pituitary, which is different from the sprung mass acceleration of the controlled output, so the short feedback control unit is designed to eliminate the difference of the controlled feedback.

4.3. Design of Endocrine Composite Skyhook-Groundhook Controller. The endocrine composite skyhook-groundhook controller consists of a skyhook-groundhook controller and endocrine controller. The output force of the skyhook-groundhook controller and the feedback sprung mass acceleration of suspension system are used as the input of the endocrine controller.

4.3.1. Design of Skyhook-Groundhook Controller. The skyhook-groundhook control strategy is the combination of skyhook control and groundhook control, which is easy to operate, fast, and robust in response. The output control force F_0 of the skyhook-groundhook control strategy is expressed as [32, 33]

$$F_0 = -c_{\text{sky}}\dot{x}_s - c_{\text{gnd}}\dot{x}_u, \tag{14}$$

where c_{sky} is the damping coefficient of skyhook control, c_{gnd} is the damping coefficient of the groundhook control, $\dot{x}_s$ is the velocity of sprung mass, and $\dot{x}_u$ is the velocity of unsprung mass.

Under different modes, the damping coefficients will determine different control effects on suspension dynamic performance and energy consumption. So, the damping coefficients of the skyhook-groundhook control under each mode are different.

4.3.2. Design of Endocrine Controller. Endocrine controller includes a long feedback control unit and short feedback control unit; the long feedback control unit consists of primary control unit and secondary control unit. The control law of each unit is designed as follows:

(1) Long feedback control unit:

The proportional adjustment is taken for the primary control unit; the output control force F_1 is expressed as

$$F_1 = F_0 + K_1 e_1 + K_2 e_3. \tag{15}$$

The deviation signal e_1 of the primary control unit is expressed as

$$e_1 = F_0 - \ddot{x}_s. \tag{16}$$

The deviation signal e_3 of the short feedback control unit is expressed as

$$e_3 = F_2 - F_0, \tag{17}$$

where K_1 is the proportional coefficient of the primary control unit, K_2 is the proportional coefficient of short feedback control unit, and F_0 is the output ideal force of different modes from the skyhook-groundhook controller.

The PID control is taken for the secondary control unit; the output control force F_2 is expressed as

$$F_2 = K_p e_2 + K_i \int e_2 \mathrm{d}t + K_d \frac{\mathrm{d}e_2}{\mathrm{d}t}. \tag{18}$$

The deviation signal e_2 for the secondary control unit is as follows

$$e_2 = F_1 - \ddot{x}_s, \tag{19}$$

where K_P, K_i, and K_d are the proportional coefficient, integral coefficient, and differential coefficient of PID control, respectively.

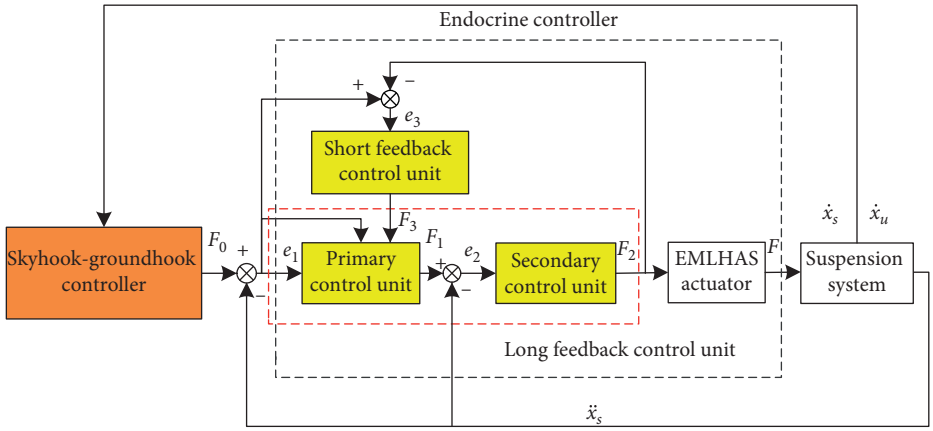

Figure 13: Control structure block diagram of endocrine composite skyhook-groundhook. F_0 is the output ideal force of different modes from the skyhook-groundhook controller, F_1 is the output control force of primary control unit, F_2 is the output control force of secondary control unit, F_3 is the output control force of short feedback control unit, F is the output control force of the EMLHAS actuator, e_1, e_2, and e_3 are the output deviation signals of primary control unit, secondary control unit, and short feedback control unit, respectively, $\dot{x}_s$ is the sprung mass velocity, and $\dot{x}_u$ is the unsprung mass velocity.

(2) Short feedback control unit:

The proportional adjustment is taken for the short feedback control unit; the output control force F_3 is expressed as

$$F_3 = K_2 (F_0 - F_2). \tag{20}$$

5. Simulation Analysis

In order to verify the effectiveness of the endocrine composite skyhook-grounghook control strategy for the EMLHAS system under different modes. The simulation analysis in time domain and frequency domain of the passive suspension, the suspension with skyhook-groundhook control strategy and the suspension with endocrine composite skyhook-groundhook control strategy, are, respectively, carried out. Also, the energy-regenerative characteristics are analyzed.

The typical working conditions in Table 3 are taken as the random road input. The simulation of economy mode, safety mode, comfort mode, and comprehensive mode are carried out successively. The time for each mode is 5 s and the total time of four modes is 20 s. The multimode random road input is obtained, as shown in Figure 14.

The initial relevant parameters of the vehicle are shown in Table 4.

The parameters of the endocrine composite skyhook-groundhook controller for each mode are finally obtained after the adjustment, which are shown in Table 5.

Firstly, the initial parameters of the vehicle given in Table 4 are taken for simulation analysis. Then, the endocrine controller parameters remain unchanged; at the same time, vehicle parameters are changed (sprung mass increased by 40% and tire stiffness decreased by 20%) for changing parameter simulation analysis to verify the adaptive performance of the endocrine composite skyhook-groundhook control strategy.

5.1. Time Domain Analysis. The time domain responses of sprung mass acceleration, suspension working space, and dynamic tire load of all types of suspension, under different modes, are obtained as shown in Figure 15. The RMS values of dynamic performance indexes and control effect of all types of suspension are as shown in Table 6.

Figure 15 and Table 6 show that, under the initial parameters simulation and changing parameters simulation, the indexes of skyhook-groundhook control and endocrine composite skyhook-groundhook control are greatly reduced, compared with the indexes of passive suspension. Also, the control effect of endocrine composite skyhook-groundhook is superior to the skyhook-groundhook control, in terms of sprung mass acceleration, suspension working space, and dynamic tire load, under different modes. For example, under the initial parameter simulation, the control of skyhook-groundhook is compared with the passive suspension, the dynamic tire load under the safety mode is reduced by 18.8%, and the sprung mass acceleration under the comfort mode is reduced by 23.6%. The same working modes are with endocrine composite skyhook-groundhook control, the dynamic tire load is reduced by 22.3% under the safety mode and the sprung mass acceleration is reduced by 28.7% under comfort mode. It can be seen that the endocrine composite skyhook-groundhook control strategy improves the vehicle riding comfort and handling stability. Meanwhile, under the changing parameter simulation, the endocrine composite skyhook-groundhook control still has good adaptability and shows superior control effect than skyhook-groundhook control, which ensures the control effect of the EMLHAS system under the condition of changing parameters.

5.2. Frequency Domain Analysis. The frequency domain resonance range of human body is 4 Hz–12.5 Hz, in which 4 Hz–8 Hz and 8 Hz–12.5 Hz are the resonance areas of the human viscera and spinal system, respectively [34]. In order

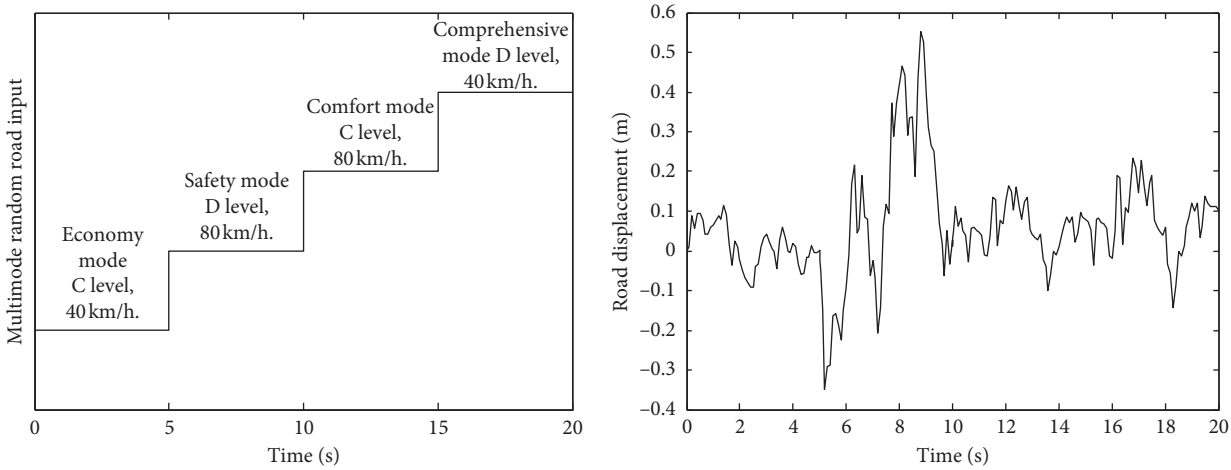

Figure 14: Multimode random road input. (a) The random road input. (b) The random road profiles.

Table 4: Initial vehicle parameters.

Parameters	Values
Sprung mass (kg)	400
Unsprung mass (kg)	37
Tire stiffness coefficient (N/m)	150000
Spring stiffness coefficient (N/m)	12000
Thrust coefficient of the linear motor (N/A)	78.54
CEMF coefficient of the linear motor ($V \cdot s \cdot m^{-1}$)	68.42
Winding resistance of the linear motor (Ω)	10.1
Lower cutoff frequency (Hz)	0.1

Table 5: Endocrine composite skyhook-groundhook controller parameters.

Working modes	Parameters						
	K_1	K_p	K_i	K_d	K_2	C_{sky}	C_{gnd}
Economy mode	2.52	0.36	0.00048	0.000012	0.66	750	550
Safety mode	2.65	0.36	0.00068	0	1.52	650	950
Comfort mode	2.56	0.358	0.0008	0.00001	0.78	1550	450
Comprehensive mode	2.55	0.38	0.0008	0	1.3	1150	650

to analyze the control effects of each strategy, from the perspective of frequency domain, the time domain results of each index, under initial parameters simulation and changing parameters simulations, are processed to obtain the average power spectral density (APSD) response, as shown in Figure 16. The highest peak values in the two resonant frequency bands are quantified. The reduction degree of the highest peak values is taken as the evaluation standard of the frequency domain analysis. The results are shown in Table 7.

Figure 16 shows that, under initial parameter simulation and changing parameter simulation, the peak values of the skyhook-groundhook control and endocrine composite skyhook-groundhook control are greatly reduced, compared with those of the passive suspension, in the human resonance frequency domain (4 Hz–12.5 Hz). In the frequency band from 12.5 Hz to 30 Hz, which is higher than that of the human resonance frequency band, there is little difference in the control effect of highest peak values between these two control strategies; the average error is less than 3%. Table 7 shows that the control effect of endocrine composite skyhook-groundhook control is better than that of skyhook-groundhook control. For example, under the initial parameter simulation and in the 4 Hz–8 Hz resonant band, the sprung mass acceleration of the skyhook-groundhook control is reduced by 33.14%, compared with that of the passive suspension. The sprung mass acceleration of the endocrine composite skyhook-groundhook control is reduced by 45.47% compared with that of the passive suspension. Other indexes are reduced with different degrees in the resonant band. The results show that the endocrine composite skyhook-groundhook control improves the vehicle riding comfort and handling stability, prevents the adverse effects of body resonance on human organs effectively, and has good adaptability under the changing parameters simulation, which ensures the control effect under the condition of changing parameters.

5.3. Energy-Regenerative Characteristic Analysis. The energy-regenerative characteristic of the EMLHAS system is expressed by the regenerative power of the linear motor. The simulation results shows that, under the initial parameters simulation, the regenerative voltage and the regenerative power of two different control strategies are respectively shown in Figures 17 and 18.

Figures 17 and 18 show that the linear motor is in the energy-regenerative state during 0–5 s. Combining with the multimode random road input in Figure 13, it can be known that this period is under the economy mode. The damping force is outputted by the solenoid valve shock absorber, and the linear motor is in the energy-regenerative state. Figure 16 shows that, under the initial parameter simulation, the peak value of regenerative voltage with two control strategies is

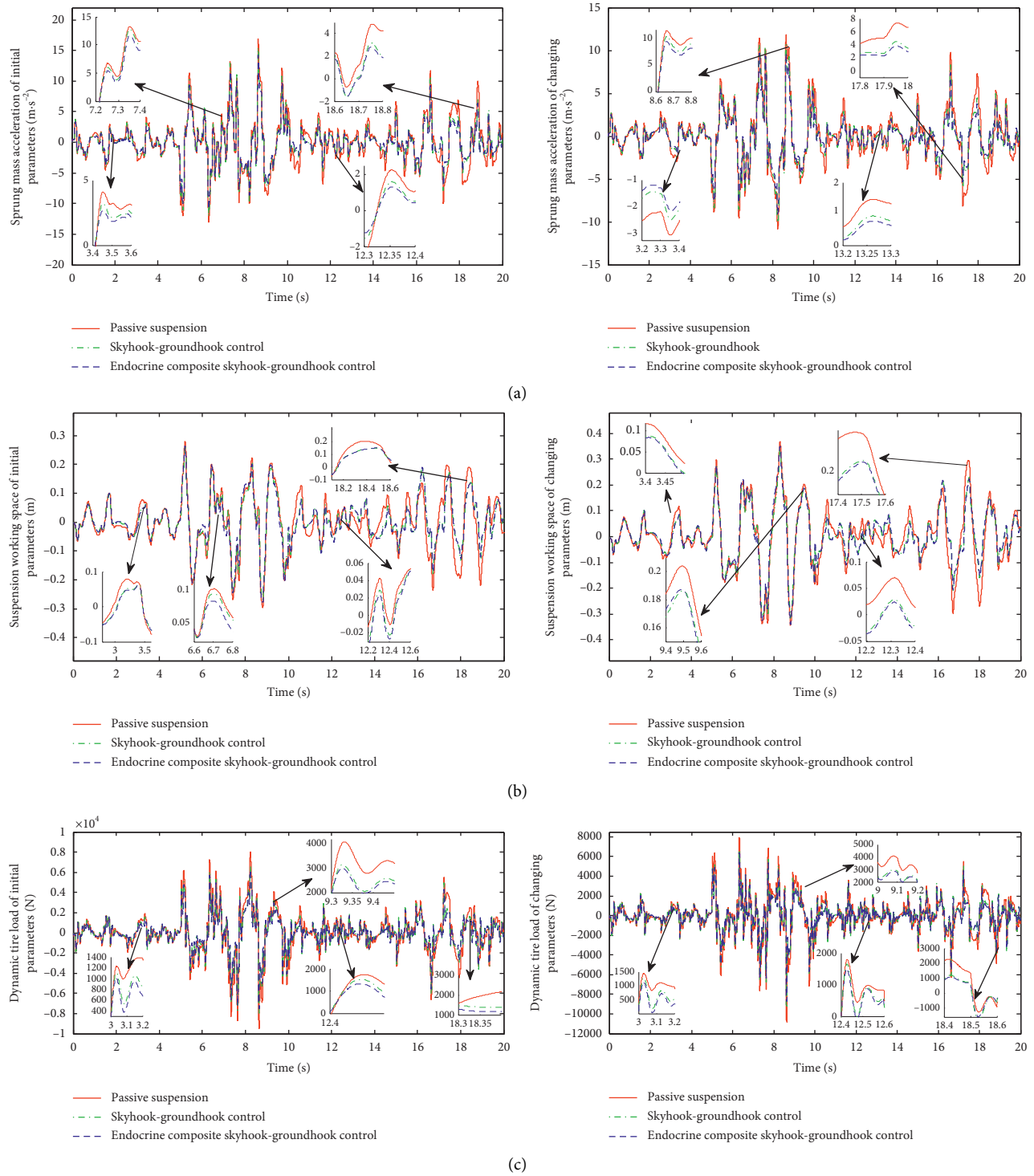

FIGURE 15: The suspension dynamic responses in time domain. (a) Time domain responses of sprung mass acceleration. (b) Time domain responses of suspension working space. (c) Time domain responses of dynamic tire load.

almost to 50 V, the difference value of average regenerative voltage is within 3%. From Figure 17, under the initial parameter simulation, the average regenerative power is 70.9 W of skyhook-groundhook control and 69.2 W of endocrine composite skyhook-groundhook control, respectively. Under the changing parameter simulation, the regenerative voltage and the average regenerative power with two control strategies are basically same. These two control strategies have little difference in energy-regenerative effects. Under the economy mode, vibration energy is recovered while the vehicle dynamic performance is guaranteed.

Table 6: The output RMS values in time domain and control effect for different suspensions.

Modes	Indexes	Initial parameters					Changing parameters				
		Suspension types			Control effect (%)		Suspension types			Control effect (%)	
		Passive	S-G	E-S-G	S-G	E-S-G	Passive	S-G	E-S-G	S-G	E-S-G
E-M	a (m·s^{-2})	1.6933	1.444	1.3935	−14.7	−17.7	1.2470	1.0774	1.0387	−13.6	−16.7
	SWS (m)	0.0404	0.0377	0.0376	−6.7	−6.9	0.0448	0.0416	0.0415	−7.1	−7.4
	DTL (N)	751.9	666.9	644.4	−11.3	−14.3	737.8	652.9	629.3	−11.5	−14.7
S-M	a (m·s^{-2})	4.7893	4.1858	4.0182	−12.6	−16.1	3.5203	3.0873	2.9605	−12.3	−15.9
	SWS (m)	0.1144	0.1076	0.1073	−5.9	−6.2	0.1266	0.1189	0.1187	−6.1	−6.2
	DTL (N)	2126.7	1726.9	1652.4	−18.8	−22.3	2083.4	1720.9	1643.8	−17.4	−21.1
C-T-M	a (m·s^{-2})	2.3945	1.8294	1.7073	−23.6	−28.7	1.7637	1.3827	1.3102	−21.6	−25.7
	SWS (m)	0.0572	0.0519	0.0517	−9.3	−9.6	0.0634	0.0574	0.0572	−9.5	−9.8
	DTL (N)	1063.4	929.4	906.0	−12.6	−14.8	1043.5	920.4	901.6	−11.8	−13.6
C-E-M	a (m·s^{-2})	3.3862	2.7902	2.5904	−17.6	−23.5	2.4936	2.0772	1.9226	−16.7	−22.9
	SWS (m)	0.0809	0.0726	0.0725	−10.2	−10.3	0.0897	0.0792	0.0791	−11.7	−11.8
	DTL (N)	1503.8	1290.3	1260.2	−14.2	−16.2	1475.7	1270.6	1229.3	−13.9	−16.7

E-M is the short form of the economy mode, S-M is the short form of the safety mode, C-T-M is the short form of the comfort mode, and C-E-M is the short form of the comprehensive mode. Also, S-G is the short form of skyhook-groundhook control and E-S-G is the short form of endocrine composite skyhook-groundhook control.

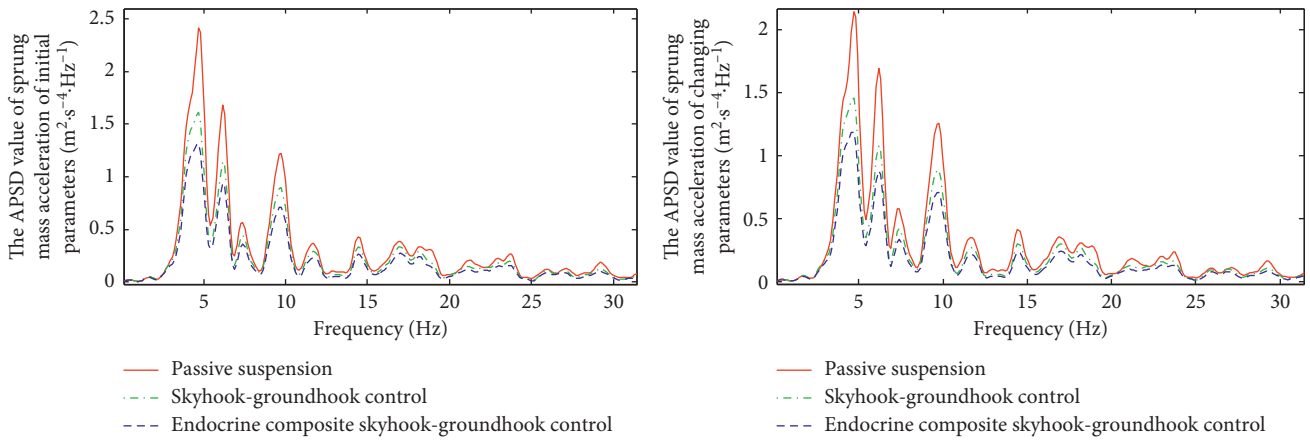

(a)

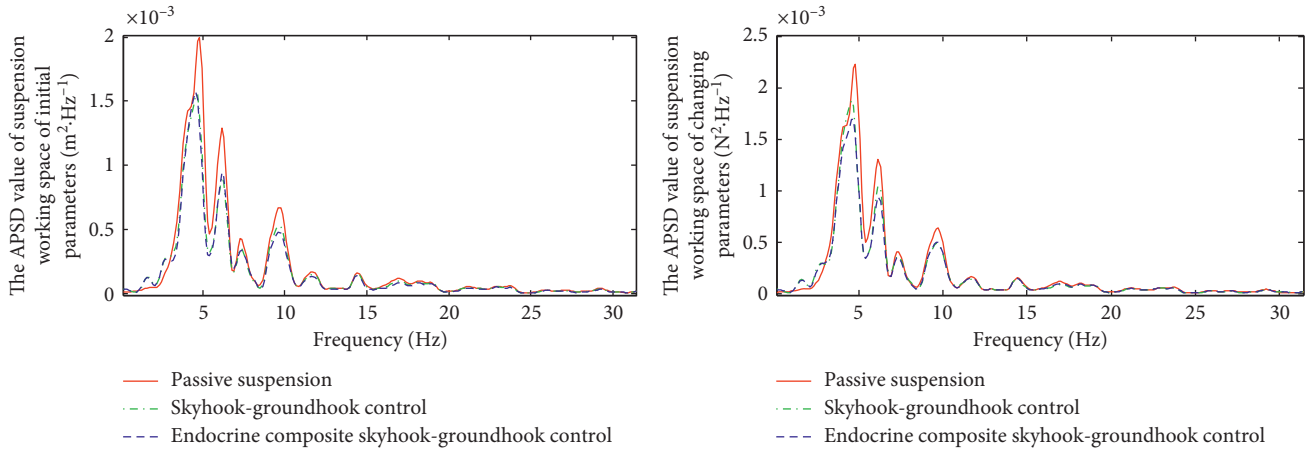

(b)

Figure 16: Continued.

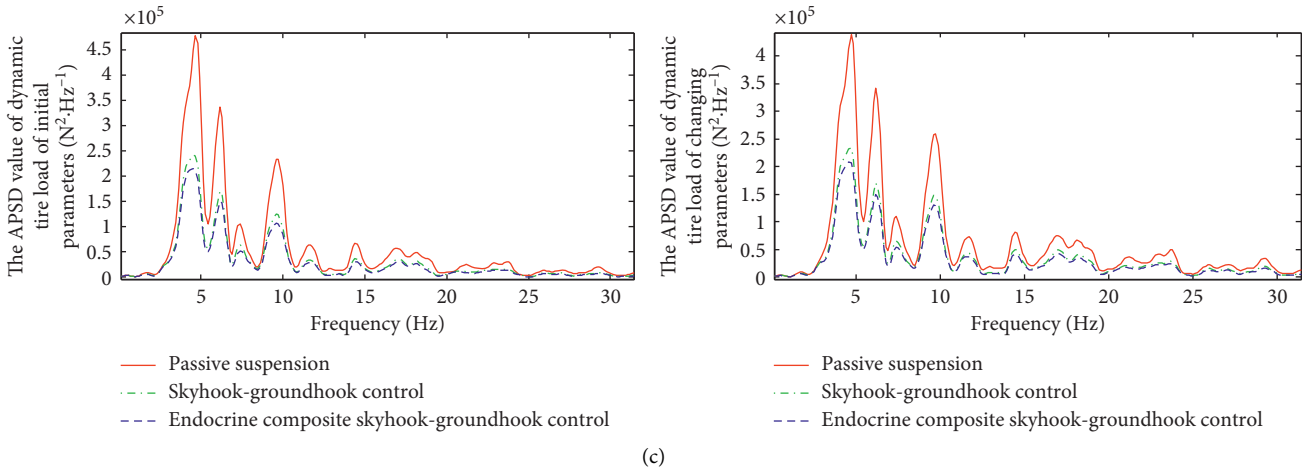

(c)

Figure 16: The suspension dynamic responses in frequency domain. (a) Frequency domain responses of sprung mass acceleration. (b) Frequency domain responses of suspension working space. (c) Frequency domain responses of dynamic tire load.

Table 7: The highest peak values quantification and control effect of the APSD value for different suspensions.

F-B (Hz)	Indexes	Initial parameters					Changing parameters				
		Suspension types			Control effect (%)		Suspension types			Control effect (%)	
		Passive	S-G	E-S-G	S-G	E-S-G	Passive	S-G	E-S-G	S-G	E-S-G
4–8	$a\,((\mathrm{m}\cdot\mathrm{s}^{-2})^2\cdot\mathrm{H}_z^{-1})$	2.417	1.616	1.318	−33.14	−45.47	2.149	1.465	1.186	−31.83	−44.81
	$\mathrm{SWS}\,(\mathrm{m}^2\cdot\mathrm{H}_z^{-1})$	1.96e−3	1.57e−3	1.56e−3	−19.89	−20.41	2.23e−3	1.82e−3	1.69e−3	−18.39	−24.22
	$\mathrm{DTL}\,(\mathrm{N}^2\cdot\mathrm{H}_z^{-1})$	4.78e5	2.41e5	2.16e5	−49.58	−54.81	4.39e5	2.33e5	2.01e5	−46.92	−54.21
8–12	$a\,((\mathrm{m}\cdot\mathrm{s}^{-2})^2\cdot\mathrm{H}_z^{-1})$	1.226	0.894	0.714	−27.08	−41.76	1.262	0.8847	0.7094	−29.89	−43.79
	$\mathrm{SWS}\,(\mathrm{m}^2\cdot\mathrm{H}_z^{-1})$	6.7e−4	5.2e−4	4.7e−4	−22.39	−29.85	6.3e−4	5.0e−4	4.9e−4	−20.63	−22.22
5	$\mathrm{DTL}\,(\mathrm{N}^2\cdot\mathrm{H}_z^{-1})$	2.34e5	1.07e5	1.06e5	−54.27	−54.70	2.59e5	1.47e5	1.31e5	−43.24	−49.42

F-B is the short form of frequency band.

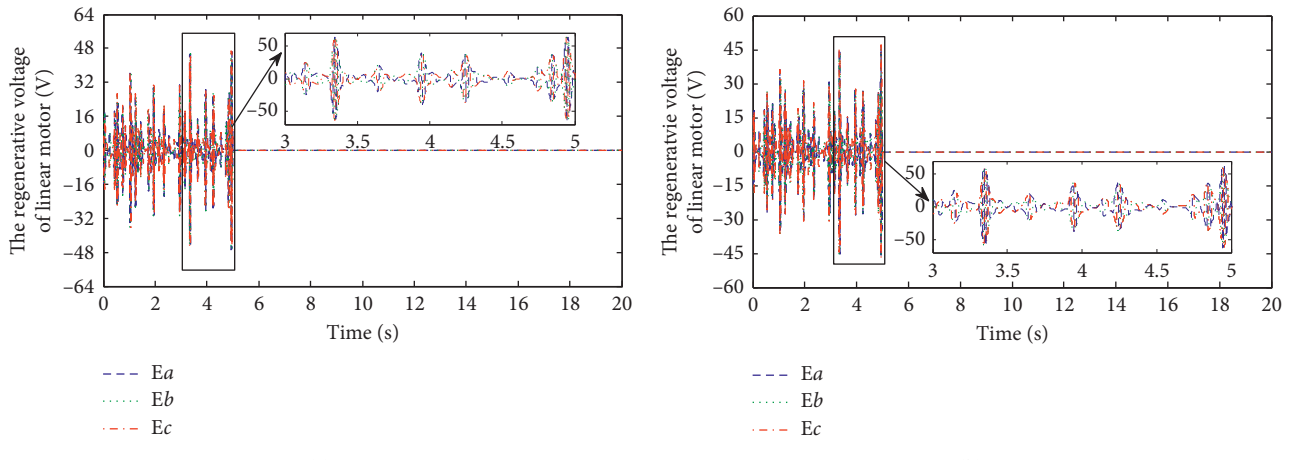

(a) (b)

Figure 17: The regenerative voltage of the linear motor with different control strategies under initial parameters. (a) The regenerative voltage with skyhook-groundhook control. (b) The regenerative voltage with endocrine composite skyhook-groundhook control.

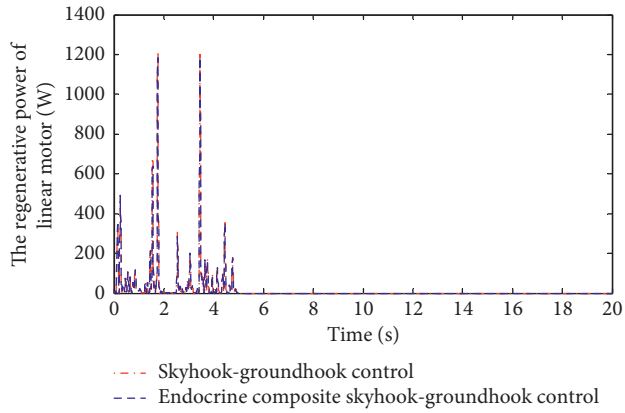

Figure 18: The regenerative power of the linear motor with different control strategies under initial parameters.

6. Conclusions

(1) A new kind of EMLHAS system is put forward, which is based on the actuator integrated with a linear motor and solenoid valve shock absorber. The mathematical models of the linear motor are found both in the active and energy-regenerative state. In addition, the force characteristic tests and the energy-regenerative characteristic tests of the linear motor are, respectively, carried out to verify the correctness of the mathematical models. At the same time, the velocity characteristic tests of the solenoid valve shock absorber are carried out to obtain the polynomial mathematical model in the semiactive state.

(2) The multimode endocrine composite skyhook-groundhook control strategy is designed for the EMLHAS system. Firstly, the suspension motion is divided into four modes according to vehicle driving conditions. Then, an endocrine control with long feedback and short feedback is combined with skyhook-groundhook control. Finally, the control laws of the skyhook-groundhook controller and endocrine controller are, respectively, designed to improve the adaptability and control effect of the control system.

(3) The simulation analysis of time domain and frequency domain is carried out by MATLAB/Simulink software. The results show the control effect of endocrine composite skyhook-groundhook control is better than that of skyhook-groundhook control and the endocrine composite skyhook-groundhook control has better adaptability to the simulation for changing parameters. The corresponding performance indexes are reduced under different modes, and the vehicle riding comfort and handling stability are improved. Under the economy mode, part of vibration energy is recovered while the vehicle dynamic performances are guaranteed.

Data Availability

The data used to support the findings of this study are available from the corresponding author upon request.

Conflicts of Interest

The authors declare that there are no conflicts of interest regarding the publication of this paper.

Acknowledgments

This work was supported by the National Natural Science Foundation of China (Grant no. 51775426), Shaanxi Provincial Key Research and Development Plan (Grant no. 2018ZDCXL-GY-05-04), and Research and Development of Applied Technology in Beilin District of Xi'an City in 2019 (Grant no. GX1928).

References

[1] M. Montazeri-Gh and O. Kavianipour, "Investigation of the active electromagnetic suspension system considering hybrid control strategy," *Proceedings of the Institution of Mechanical Engineers, Part C: Journal of Mechanical Engineering Science*, vol. 228, no. 10, pp. 1658–1669, 2014.

[2] W. Sun, Y. Zhao, J. Li, L. Zhang, and H. Gao, "Active suspension control with frequency band constraints and actuator input delay," *IEEE Transactions on Industrial Electronics*, vol. 59, no. 1, pp. 530–537, 2011.

[3] H. E. Tseng and D. Hrovat, "State of the art survey: active and semi-active suspension control," *Vehicle System Dynamics*, vol. 53, no. 7, pp. 1034–1062, 2015.

[4] F. Kou, J. Du, Z. Wang, D. Li, and J. Xu, "Nonlinear modeling and coordinate optimization of a semi-active energy regenerative suspension with an electro-hydraulic actuator," *Algorithms*, vol. 11, no. 2, 2017.

[5] J. Liu, X. Li, Z. Wang, and Y. Zhang, "Modelling and experimental study on active energy-regenerative suspension structure with variable universe fuzzy PD control," *Shock and Vibration*, vol. 2016, Article ID 6170275, 11 pages, 2016.

[6] J. Liu, X. Li, X. Zhang, and X. Chen, "Modeling and simulation of energy-regenerative active suspension based on BP neural network PID control," *Shock and Vibration*, vol. 2019, Article ID 4609754, 8 pages, 2019.

[7] S. Chen, X. Li, L. Zhao, Y. Wang, and Y. Kim, "Development of a control method for an electromagnetic semi-active suspension reclaiming energy with varying charge voltage in steps," *International Journal of Automotive Technology*, vol. 16, no. 5, pp. 765–773, 2015.

[8] L. Chen, D. Shi, R. Wang, and H. Zhou, "Energy conservation analysis and control of hybrid active semi-active suspension with three regulating damping levels," *Shock and Vibration*, vol. 2015, Article ID 6196542, 14 pages, 2015.

[9] B. Huang, C. Y. Hsieh, F. Golnaraghi, and M. Moallem, "Development and optimization of an energy-regenerative suspension system under stochastic road excitation," *Journal of Sound and Vibration*, vol. 357, pp. 16–34, 2015.

[10] F. Kou, D. Wei, and L. Tian, "Multimode coordination control of a hybrid active suspension," *Shock and Vibration*, vol. 2018, Article ID 6378023, 16 pages, 2018.

[11] R. Ding, R. Wang, and X. Meng, "Energy-saving control strategy design and structure realization for electromagnetic active suspension," *Proceedings of the Institution of Mechanical Engineers, Part C: Journal of Mechanical Engineering Science*, vol. 233, no. 9, pp. 3060–3075, 2019.

[12] R. Wang, Y. Qian, R. Ding, X. Meng, and J. Xie, "Damping-stiffness design and experimental study of hybrid electromagnetic suspension based on LQG," *Journal of Vibration and Shock*, vol. 37, no. 3, pp. 61–65, 2018.

[13] H. Peng, J. Zhang, J. Zhang, D. Huang, and C. Han, "Study on model reference multi-mode switching control of parallel composite electromagnetic suspension," *Journal of Military Engineering*, vol. 40, no. 1, pp. 19–28, 2019.

[14] Y. Hu, M. Chen, and Y. Sun, "Comfort-oriented vehicle suspension design with skyhook inerter configuration," *Journal of Sound and Vibration*, vol. 405, pp. 34–47, 2017.

[15] Y. Kang, H. Pang, K. Liu, J. Yang, and X. Chai, "Skyhook control of multi-stage adjustable damp semi-active air suspension," *Mechanical Science and Technology for Aerospace Engineering*, vol. 35, no. 5, pp. 778–783, 2016.

[16] Z. Li, L. Ju, H. Jiang, and X. Xu, "Imitated skyhook control of a vehicle laterally interconnected air suspension," *International Journal of Vehicle Design*, vol. 74, no. 3, pp. 204–230, 2017.

[17] J. Zhang, D. Huang, and Y. Liu, "Improved semi-active control algorithm on groundhook and its performance analysis," *Journal of Huazhong University of Science and Technology*, vol. 45, no. 4, pp. 84–89, 2017.

[18] T. Yan, D. Liu, Z. Shi, H. Chen, and B. Chen, "Simulation of road friendliness of semi-active suspension vehicle based on groundhook control," *Chinese Journal of Agricultural Machinery*, vol. 38, no. 1, pp. 12–16+11, 2007.

[19] K. Guo, J. Sui, and Y. Guo, "Semi-active control of high-speed vehicle lateral shock absorber based on mixed damping of skyhook and groundhook," *Vibration and Impact*, vol. 32, no. 2, pp. 18–23, 2013.

[20] C. Sauze and M. Neal, "Artificial endocrine controller for power management in robotic systems," *IEEE Transactions on Neural Networks and Learning Systems*, vol. 24, no. 12, pp. 1973–1985, 2013.

[21] M. Milovanović, D. Antić, M. Milojković, S. Nikolić, S. Perić, and M. Spasić, "Adaptive PID control based on orthogonal endocrine neural networks," *Neural Networks*, vol. 84, pp. 80–90, 2016.

[22] X. Liang, Y. Ding, L. Ren, K. Hao, and Y. Jin, "Data-driven cooperative intelligent controller based on the endocrine regulation mechanism," *IEEE Transactions on Control Systems Technology*, vol. 22, no. 1, pp. 94–101, 2013.

[23] S. Shu, X. Wang, H. Xia, and C. Yu, "Design of intelligent controller based on neuroendocrine algorithm," *Journal of Electronic Measurement and Instrumentation*, vol. 32, no. 7, pp. 192–197, 2018.

[24] Y. Jin, D. Yu, Z. Chen, M. Jiang, and X. He, "Endocrine LQR control strategy and active suspension vibration reduction research," *Journal of Vibration and Shock*, vol. 35, no. 10, pp. 49–54, 2016.

[25] I. Martins, J. Estevez, and G. Marques, "Permanent-magnets linear actuators applicability in automobile active suspensions," *IEEE Transactions on Vehicular Technology*, vol. 55, no. 1, pp. 86–94, 2006.

[26] L. Chai and T. Sun, "The design of LQG controller for active suspension based on analytic hierarchy process," *Mathematical Problems in Engineering*, vol. 2010, Article ID 701951, 19 pages, 2010.

[27] L. Yang, D. Chen, Z. Gao, and Y. Chen, "Nonlinear control of one quarter vehicle semi-active suspension based on solenoid valve shock absorber," *Chinese Journal of Agricultural Machinery*, vol. 45, no. 4, pp. 1–7, 2014.

[28] J. Si, H. Wang, X. Xu, and H. Feng, *Modeling, Characteristic Analysis and Thrust Control of PMLSM*, China University of Mining and Technology Press, Xuzhou, China, 2014.

[29] J. Wang, W. Wang, and K. Atallah, "A linear permanent-magnet motor for active vehicle suspension," *IEEE Transactions on Vehicular Technology*, vol. 60, no. 1, pp. 55–63, 2010.

[30] A. Thul, D. Eggers, B. Riemer, and K. Hameyer, "Active suspension system with integrated electrical tubular linear motor: design, control strategy and validation," *Archives of Electrical Engineering*, vol. 64, no. 4, pp. 605–616, 2015.

[31] A. J. Tiblbrook and I. J. Clarke, "Neuroendocrine mechanisims of innate states of attenuated responsiveness of the hypothalamo-pituitary adrenal axis to stress," *Frontiers in Neuroendocinology*, vol. 27, no. 3, pp. 285–307, 2006.

[32] Y. Qin, M. Dong, R. Langari, L. Gu, and J. Guan, "Adaptive hybrid control of vehicle semi-active suspension based on road profile estimation," *Shock and Vibration*, vol. 2015, Article ID 636739, 13 pages, 2015.

[33] S. Han, Z. Chao, and X. Liu, "A semi-active and adaptive hybrid control system for a tracked vehicle hydropneumatic suspension based on disturbance identification," *Shock and Vibration*, vol. 2017, Article ID 2741786, 12 pages, 2017.

[34] Z. Yu, *Automobile Theory*, China Machine Press, Beijing, China, 2009.